**SANDIA REPORT**

SAND2011-6770
Unlimited Release
Printed October 2011

# High-Pressure Shock Behavior of WC and $Ta_2O_5$ Powders

Tracy J. Vogler, Seth Root, Marcus D. Knudson, William D. Reinhart

Prepared by
Sandia National Laboratories
Albuquerque, New Mexico 87185 and Livermore, California 94550

Sandia National Laboratories is a multi-program laboratory managed and operated by Sandia Corporation, a wholly owned subsidiary of Lockheed Martin Corporation, for the U.S. Department of Energy's National Nuclear Security Administration under contract DE-AC04-94AL85000.



Issued by Sandia National Laboratories, operated for the United States Department of Energy by Sandia Corporation.



Available to DOE and DOE contractors from
U.S. Department of Energy
Office of Scientific and Technical Information
P.O. Box 62
Oak Ridge, TN 37831

Telephone: (865) 576-8401
Facsimile: (865) 576-5728
E-Mail: reports@adonis.osti.gov
Online ordering: http://www.osti.gov/bridge

Available to the public from
U.S. Department of Commerce
National Technical Information Service
5285 Port Royal Rd
Springfield, VA 22161

Telephone: (800) 553-6847
Facsimile: (703) 605-6900
E-Mail: orders@ntis.fedworld.gov
Online ordering: http://www.ntis.gov/help/ordermethods.asp?loc=7-4-0#online

SAND2011-6770
Unlimited Release
Printed October 2011

# High-Pressure Shock Behavior of WC and $Ta_2O_5$ Powders

Tracy J. Vogler
Sandia National Laboratories
7011 East Ave.
M.S. 9042
Livermore, CA 94550

Seth Root, Marcus D. Knudson, William D. Reinhart
Sandia National Laboratories
P.O. Box 5800
M.S. 1195
Albuquerque, NM 87185

**Abstract**

Planar shock experiments were conducted on granular tungsten carbide (WC) and tantalum oxide ($Ta_2O_5$) using the Z machine and a 2-stage gas gun. Additional shock experiments were also conducted on a nearly fully dense form of $Ta_2O_5$. The experiments on WC yield some of the highest pressure results for granular materials obtained to date. Because of the high distention of $Ta_2O_5$, the pressures obtained were significantly lower, but the very high temperatures generated led to large contributions of thermal energy to the material response. These experiments demonstrate that the Z machine can be used to obtain accurate shock data on granular materials. The data on $Ta_2O_5$ were utilized in making improvements to the P-$\lambda$ model for high pressures; the model is found to capture the results not only of the Z and gas gun experiments but also those from laser experiments on low density aerogels. The results are also used to illustrate an approach for generating an equation of state using only the limited data coming from nanoindentation. Although the EOS generated in this manner is rather simplistic, for this material it gives reasonably good results.

# Acknowledgment

The authors wish to thank the large team at Z for the execution of the experiments there, Dustin Romero and Jeff Gluth for the design and filling of the Z test hardware, and the team at STAR - Heidi Anderson, John Martinez, Tom Thornhill, and Robert (Rocky) Palomino - for the execution of the gas gun experiments. We would also like to thank Dennis Grady and Gregg Fenton of Applied Research Associates for the use of their EOS results and Tom Buchheit for the nanoindentation results on $Ta_2O_5$.

Sandia National Laboratories is a multi-program laboratory operated by Sandia Corporation, a wholly owned subsidiary of Lockheed Martin company, for the U.S. Department of Energy's National Nuclear Security Administration under contract DE-AC04-94AL85000.

# Contents



# Figures

# Tables

# 1 Introduction

Development of an equation of state (EOS) for a material is an involved undertaking. Accurate experimental data over a wide range of thermodynamic conditions is an essential part of EOS development. Historically, shock (Hugoniot) data represented a key form of experimental data for EOS calibration at high pressures (c.f. [Marsh, 1980; Trunin et al., 2001]). The principal Hugoniot, however, often does not serve as a strong constrain [Knudson et al., 2005] for EOS development. It is possible that many EOSs can match the principal Hugoniot, but differ substantially from one another in off-Hugoniot states. One can examine release states [Knudson et al., 2005], non-shock thermodynamic states [Davis, 2006], or shocked states for initially porous materials [Trunin et al., 1989]. The last of these, which has been especially common in Russian and Soviet research, utilizes the extra dissipative work associated with the lower initial density to reach states that can be much hotter than those on the principal Hugoniot for a given pressure. The study of porous samples has the advantage of utilizing relatively standard shock physics techniques, and by controlling the initial density of the material one can probe a very wide range of thermodynamic states.

In this report, we extend our previous work on the compaction of granular ceramics [Brown et al., 2007; Vogler et al., 2007] to the high-pressure regime to obtain stresses of over 400 GPa in tungsten carbide and 150 GPa in tantalum pentoxide using a two-stage gas gun and the Z machine. Tungsten carbide has been studied extensively through low pressure compaction [Vogler et al., 2007], pressure-shear loading [Vogler et al., 2011], and mesoscale modeling [Borg and Vogler, 2008, 2009]. Tantalum pentoxide was available in granular forms that gave two significantly different pour densities so that a broader range of thermodynamic space could be spanned. Also, it has been studied previously in aerogel form [Miller et al., 2007]; such aerogels are primarily of interest for their use in various laser-driven experiments [Hibbard and Bono, 2005; Hund et al., 2006].

This page intentionally left (almost) blank.

# 2 Experimental techniques

## 2.1 Materials

Two ceramic compounds were the subject of this investigation: tungsten carbide (WC) and tantalum pentoxide ($Ta_2O_5$). A single form of granular WC was studied, while granular $Ta_2O_5$ from two different sources were studied along with a partially consolidated form.

#### Cerac $Ta_2O_5$

The first version of $Ta_2O_5$ studied was purchased from Cerac Inc. (now known as Materion) and is shown in Fig. 1. This and the other varieties were found to have an orthorhombic structure through X-ray diffraction measurements. The Cerac material is characterized by significant porosity at the scale of the grain as seen in Fig. 1a and porosity at the sub-grain level as seen in Fig. 1b. The two levels of porosity lead to a very low pour density for the material, approximately 1.1-1.2 g/cm$^3$, compared to the theoretical density of 8.2 g/cm$^3$. The quoted purity of this material was 99.5%, and the particle sizes were nominally greater than 44 $\mu$m and less than 149 $\mu$m.

#### American Elements $Ta_2O_5$

The second version of $Ta_2O_5$ was purchased from American Elements and is shown in Fig. 2. The subscale porosity shown in Fig. 2b is similar to that of the Cerac material, but this material tends to be ellipsoidal in shape without grain-scale porosity. As a result, pour densities for this material were significantly higher, approximately 3.0 g/cm$^3$. The quoted purity of this material was 99.99%, and the mean particle sizes was 30 $\mu$m. Almost all particles were less than 60 $\mu$m, and there was a modest amount of particles smaller than 10 $\mu$m. No information is available on what processing parameters led to the formation of the particle structures of the Cerac material as opposed to the American Elements material.

#### Consolidated $Ta_2O_5$

The third version of $Ta_2O_5$ was purchased in the form of partially consolidated disks from American Elements. The disks were nominally 20 mm in diameter and approximately 3.2 mm thick. Their density was 7.4-7.5 g/cm$^3$, or 90-91% of the crystalline density. The quoted purity of this material was 99.9%.

#### Kennametal WC

The final material studied was a macro crystalline variety [Lassner and Schubert, 1999] of tungsten carbide produced by Kennametal, Inc. The compaction response of this material has been reported previously [Vogler et al., 2007]. As shown in the SEM image in Fig. 3, each grain is an individual single crystal. Sieving of the material gave grains of 20-32 $\mu$m in size.

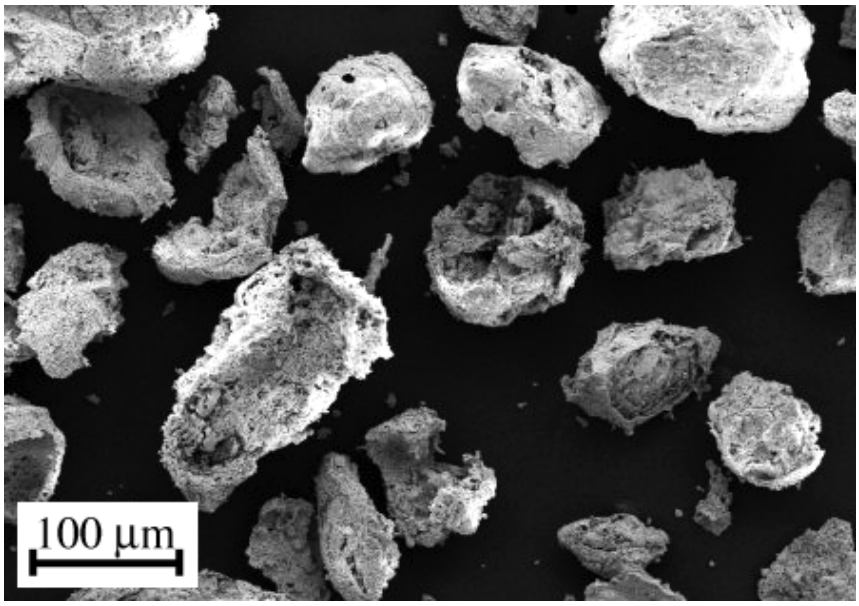


**(a)**

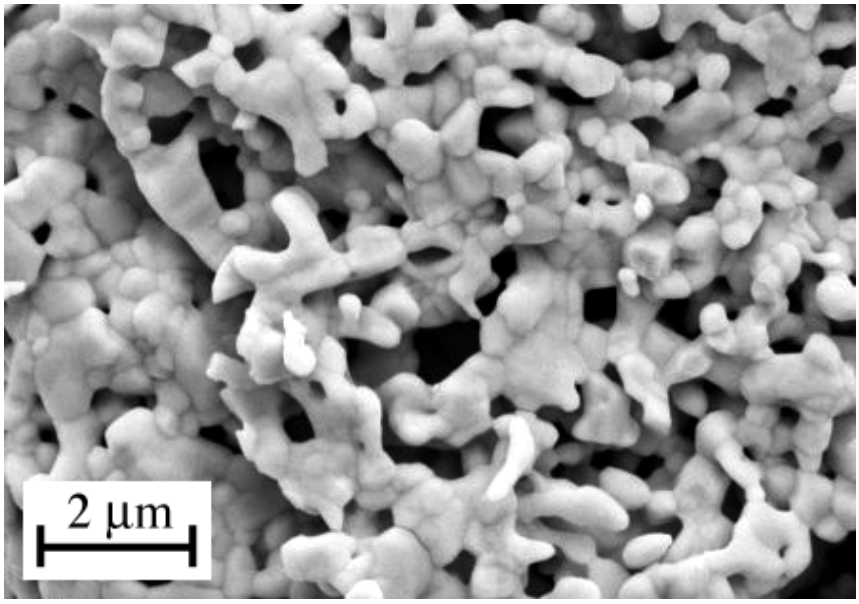


**(b)**

**Figure 1.** SEM micrographs of $Ta_2O_5$ from Cerac showing (a) grain structure and (b) sub-grain structure.

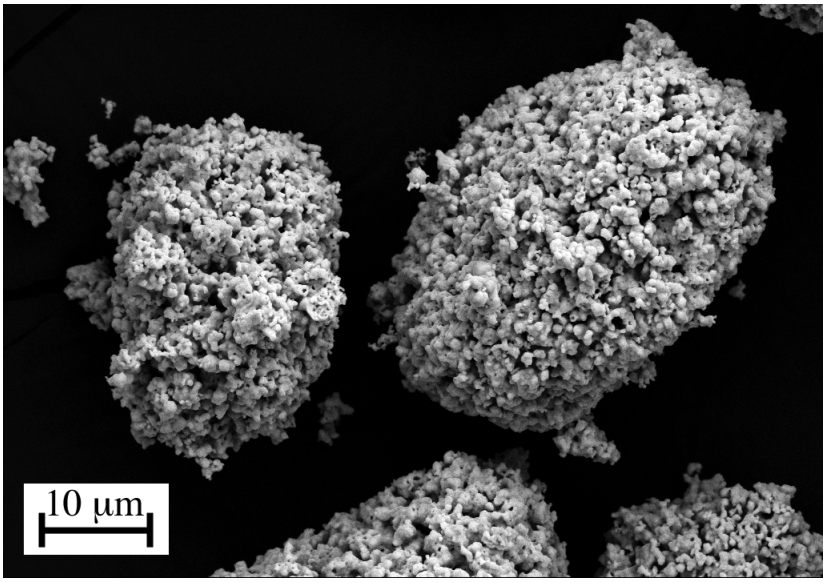


**(a)**

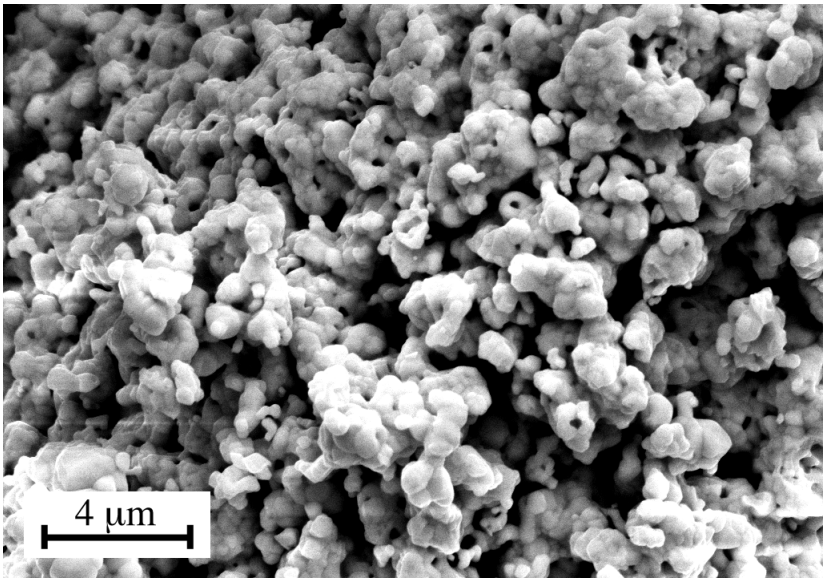


**(b)**

**Figure 2.** SEM micrographs of $Ta_2O_5$ from American Elements showing (a) grain structure and (b) sub-grain structure.

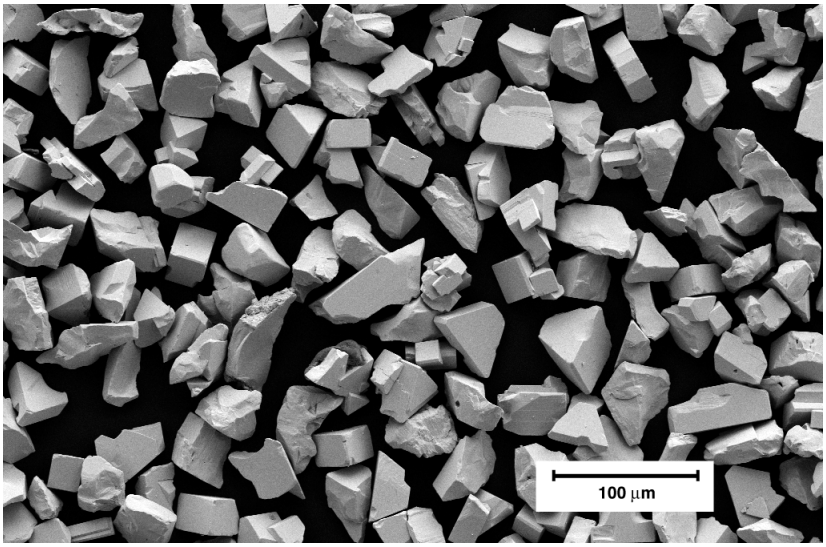


**Figure 3.** SEM micrographs of WC from Kennametal.

## 2.2 Configuration for Z Experiments

Planar shock experiments were conducted on Sandia's Z machine [Hall et al., 2001]. The large currents generated by Z are used to launch flyer plates at velocities far above those achievable using conventional gas gun techniques [Knudson et al., 2001]. The experimental configuration used for the experiments, shown in Fig. 4, is similar to that used by [Knudson et al., 2001] with some features of the cell used by [Vogler et al., 2007].

A current of approximately 12 MA flows up the anode and down the cathode as shown in the inset of the figure. These currents induce a magnetic field between the cathode and anode, and the interaction between this field and the current produces mechanical stress waves through Lorentz forces that are proportional to the current squared. The stress waves accelerate the 700 $\mu$m thick aluminum anode layer which pushes a 300 $\mu$m thick copper impactor, which flies across the gap and hits the 300 $\mu$m thick copper "driver." Because the anode and impactor are accelerated by smooth waves rather than shock waves, loading is nearly isentropic so that impact with the driver is approximately symmetric. There is, of course, some dissipation through plasticity and other mechanisms, but those effects will be ignored here. Five VISAR [Barker and Hollenbach, 1972] probes monitor the impactor along its length so that the impact velocity and timing along the vertical direction can be accurately determined. The left and right anodes are placed at different distances from the cathode (an asymmetric A-K gap), resulting in slightly different impact velocities, here about 11 km/s for the narrower gap versus 10 km/s for the wider gap.

The sample cell consists of a single cavity cut out of the copper driver with a Lexan covering it to contain the powder. Different views of the copper driver piece and the Lexan cover are shown in Fig. 5. Four circular regions with diameters of 8 mm are diamond turned in the driver, and z-cut quartz windows (6 mm diameter

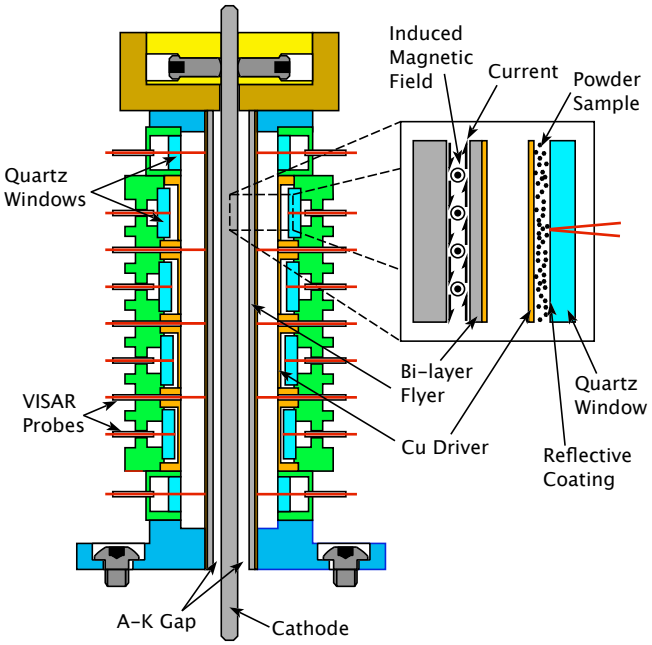


**Figure 4.** Schematic view of the experiments on the Z machine with inset showing the details of the current flow, magnetic field, and powder sample.

and 1.5 mm thick) were attached to the Lexan cover above each at different distances, nominally 400, 600, 800, and 1000 $\mu$m. Measurements of the parts are made prior to filling to ensure that the sample thicknesses and the sample volume are known accurately. A thin reflective layer of aluminum is deposited on each of these windows for use with VISAR diagnostics. After the Lexan cover is attached to the copper driver, the cavity is filled with WC or $Ta_2O_5$ powder. Filled capsules are shown in Fig. 6. Measuring the mass of the cell prior to and after filling provides the mass of the sample. A vent hole filled with a porous filter allows gas to vent from the sample when the target chamber at Z is evacuated without losing material. The five VISAR probes monitoring the flyer consist of three fiber probes through the cover and driver as well as two probes above and below the sample looking through quartz windows (no reflective coating) at the flyer.

Impact of the flyer generates a shock that travels through the driver and into the powder sample. The shock travels through the sample and reaches the sample / window interface where the VISAR diagnostics measure the time of shock arrival. The four different shock arrival times provide an accurate measurement of the shock velocity $U_s$. In principal, as the shock travels through the quartz window it should be reflective allowing measurement of $U_s$ in the window, which would provide a reshock or release state for the sample. After impact, the shock also travels through the impactor until it reaches the flyer / anode interface, resulting in a release wave that will travel back into the sample. From the time when this release overtakes the shock in the quartz window it should be possible to determine the release wave speed of the sample.

## 2.3 Configuration for Gas Gun Experiments

Planar impact experiments were also conducted on a 28 mm bore two-stage light gas gun at impact velocities up to 6.5 km/s. All three forms of $Ta_2O_5$ were tested in this manner. The same basic configuration shown in Fig. 7 was used for both of the powders, while a modified version discussed below was used for the consolidated material.

A copper or aluminum impactor is launched on a Lexan projectile. Its velocity is measured to an accuracy of 0.2% using an optical system. The impactor strikes a driver plate that is approximately 1 mm thick and made of the same material. This generates a shock that travels through the driver into the powder sample, which consists of a stepped target made of two cylindrical spaces cut from a PMMA block that is attached to the driver plate. The target is filled through a hole in the PMMA block, and a vent hole with a porous ceramic filter allows it to vent to the evacuated target chamber. Each step of the target is approximately 0.75 mm thick. VISAR probes are used to monitor the arrival of the shock at the back of the driver plate, at the back of the first (outer) step, and at the back of the second (inner) step. Arrival times for the shock waves at these three thicknesses were used to calculate a shock velocity, $U_s$, for the experiment. The use of probes on opposite sides of the target makes it possible to correct for the effects of tilt, but any bowing of the impactor that might be occurring cannot be measured. In some experiments, small LiF windows with thin ( 0.25 mm) Al buffers were incorporated into the PMMA block to allow for better measurement of the wave profiles in the samples.

The setup for consolidated $Ta_2O_5$ differs somewhat from that for powder samples and is shown schematically in Fig. 8. For some of the experiments, the Cu impactor directly struck the target, while in others a Cu driver plate approximately 0.8 mm thick was in front of the sample. This driver plate was useful in reducing possible effects due to small amounts of gas ahead of the impactor. The samples were cylindrical disks 20 mm in diameter and approximately 3.2 mm thick. Two small LiF windows flanked the sample, and a

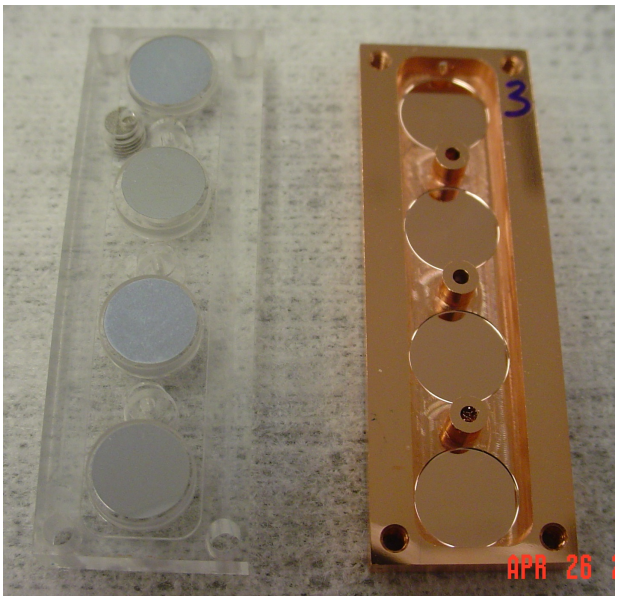


**(a)**

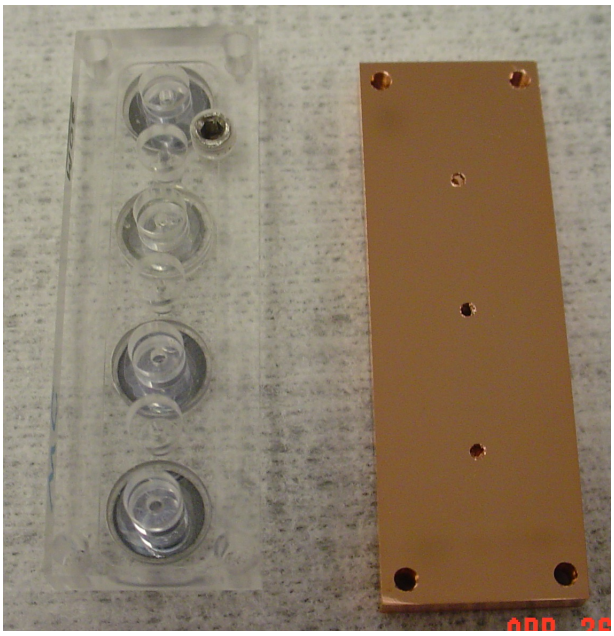

**(b)**

**Figure 5.** Views of the Lexan cover and the copper driver piece prior to assembly showing (a) the interior and (b) the exterior of each.

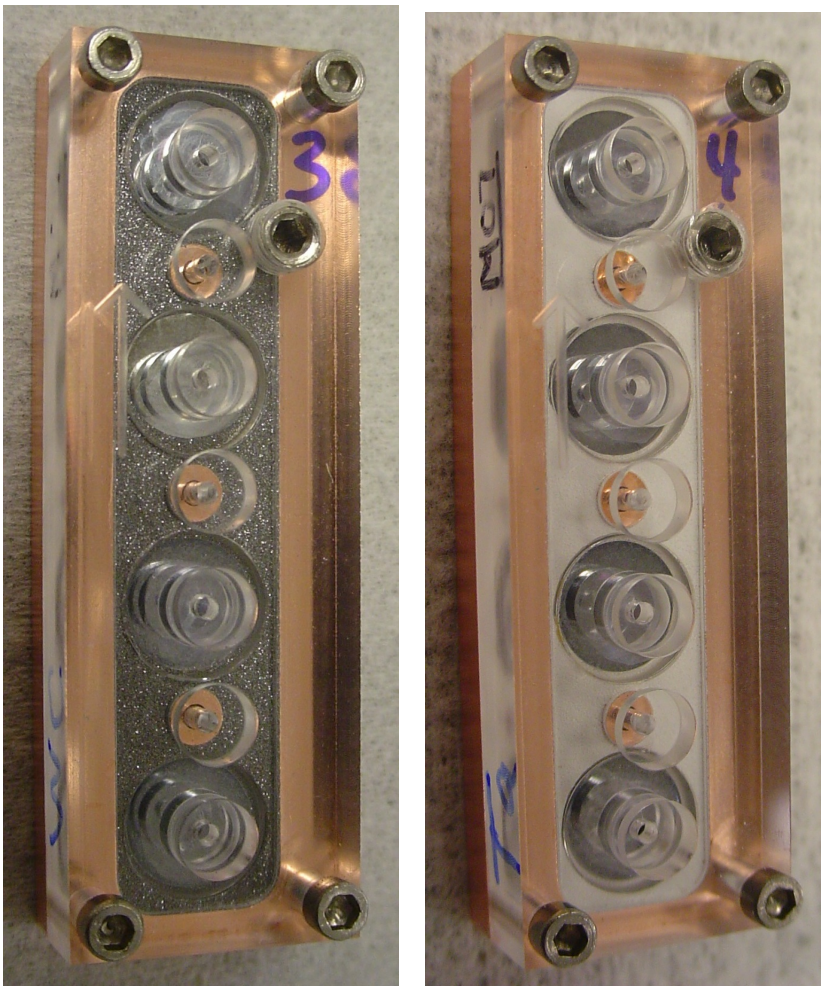

**(a)** **(b)**

**Figure 6.** Assembled capsules filled with (a) WC and (b) $Ta_2O_5$ powder.

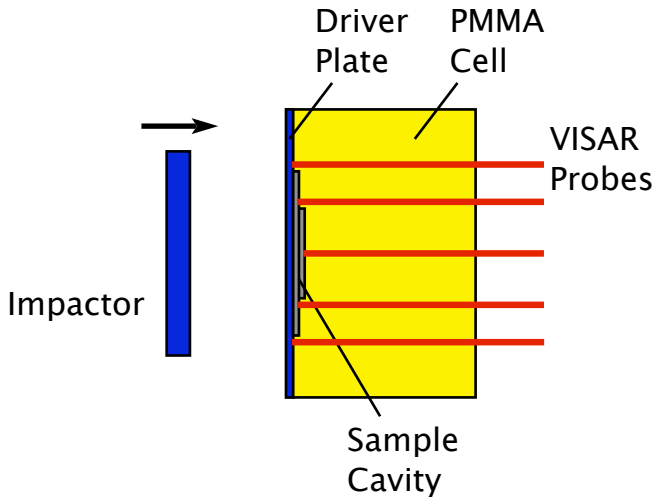


**Figure 7.** Schematic of the target used in 2-stage gas gun experiments.

third larger window was affixed to the back of the sample. The front surfaces of these windows, which were coated with a thin reflective layer of aluminum, were monitored using VISAR. In order to protect the reflective surface and thus provide a longer read time for the VISAR probe on the center window, a thin (0.25 mm) thick Al buffer was placed between the sample and the window.

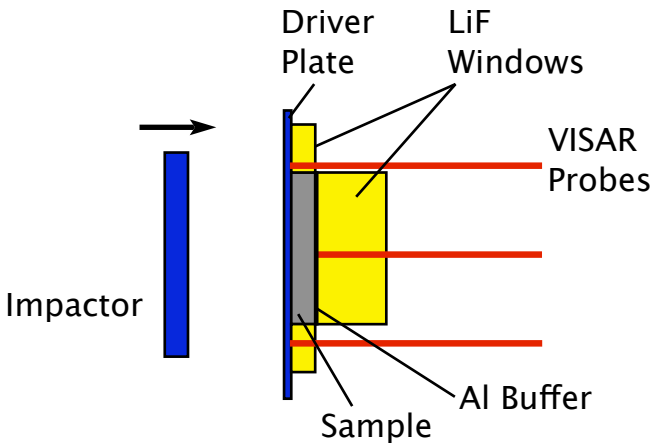


**Figure 8.** Schematic of the target used in 2-stage gas gun experiments on consolidated $Ta_2O_5$.

# 3 Results for Z Experiments

Results from two Z experiments are presented in this section. The analysis of these experiments was complicated by the difficulty in determining an impact time on the copper buffer. Velocity histories as measured through one of the quartz windows and two of the central fiber probes are shown in Fig. 9. The velocities are relatively consistent for the three measurements, though each of the records becomes erratic at somewhat different times. In part, this is due to the inevitable tilt that occurs during the experiment where the bottom of the flyer impacts somewhat later than the top. Tilt can be accounted for in a relatively straightforward manner, but a more significant problem is encountered when the velocity histories from the fiber probes are examined. When the flyer impacts the quartz window, it generates an unambiguous signal in the VISAR record as shown in the inset of Fig. 9. In contrast, the impact of the flyer with the fiber probes between the powder samples does not give a "clean" signal that can be reliably interpreted as impact time. This is because the send and receive fibers are parallel but offset from one another, and as the flyer gets close to their ends very little light is returned. Even in the raw data signals, no clear indication of impact was observed in the VISAR signal from the probes along the copper powder cell. Lacking a clear fiducial, these fiber probes cannot be used for determination of impact time.

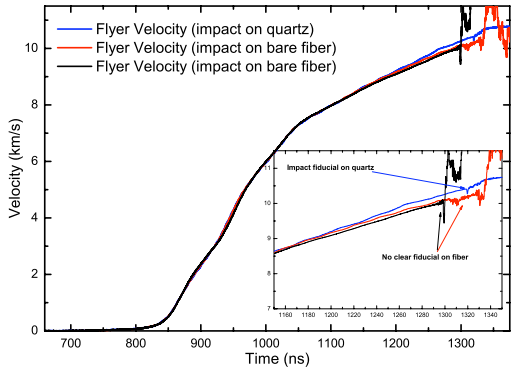


**Figure 9.** Velocity history records for flyer plate launch on experiment Z-2157. Shown in the inset are the velocity records near the time of impact. Although the black curve shows a large velocity jump at around 1300 ns, it cannot be directly tied to impact.

A second issue that compounded the difficulty in the data analysis was that no measurements were made of the offset distance between the impact surface of the quartz windows and the impact surface of the copper powder cells. Also not measured was the tilt (or equivalently flight distance) of the copper powder cell after it was epoxied into the anode panel frame. The Lexan back cover had all VISAR fiber optics connected prior to attaching the cover to the copper powder cell, making any offset or tilt measurements difficult. Thus the data analysis assumes that both quartz windows' and the target cell's impact surface are all in the same plane. Although the quartz windows and copper powder cell are assembled on a granite flat, the presence of a piece of dust or changes in shape during setting of the epoxy can result in small offsets of those pieces. Measurements in previous experiments indicate that offsets of 20 $\mu$m or more are possible.

The shock velocity of the powder samples is determined through transit time analysis. Impact time along the copper cell is determined by interpolating impact times from the two quartz windows and assuming that the average velocity determined from the flyer measurements at the two quartz window locations holds across the entire target cell. The shock arrival at the powder/quartz interface is determined from the raw VISAR signal to typically within 0.1 ns. The shock arrival times at the powder/quartz interfaces are adjusted for flyer tilt and copper counterbore thickness. The resulting arrival times are then plotted versus powder sample thickness. The slope of the least squares linear fit to the data (thickness vs. transit time) determines the inverse of the shock velocity and the slope uncertainty of the fit gives the shock velocity uncertainty. The Hugoniot state is calculated using a *Monte Carlo* impedance match method [Root et al., 2010] with a reflected copper Hugoniot.

The *Monte Carlo* impedance matching technique provides a method to propagate uncertainties from experimentally measured values and the Hugoniot standards into the final results. The method proceeds as follows:

- Experimentally measured quantities (flyer velocity, initial density, shock velocity, etc.) are varied about their mean value by multiplying the uncertainties with uncorrelated random numbers that have a standard deviation of 1 and a mean of 0.
- The copper Hugoniot $U_S - u_p$ fit parameters are varied about their mean value using correlated random numbers determined from a reanalysis of existing copper Hugoniot data. (Briefly, a weighted *Monte Carlo* method was used to calculate fit parameters and the covariance matrix of the parameters to existing copper data). A reflection of the copper Hugoniot is used for the release path.
- The powder Hugoniot state is determined using the standard impedance matching calculation as shown schematically in Fig. 10.
- The process is repeated (typically $10^6$ calculations) to build a large statistical distribution of Hugoniot states for the powder. The final state is the mean value of the distribution and the uncertainty is taken as 1 standard deviation of the distribution.

The Z experimental results are listed in Table 1. Note that uncertainties due to possible offsets of the quartz and copper panel impact surfaces are not included in the uncertainties shown in the table.

**Table 1.** Details of materials and Hugoniot states for Z experiments.

| *Shot* | *Material* | $\rho_{oo}$ *(g/cm$^3$)* | $V_{impact}$ *(km/s)* | $U_s$ *(km/s)* | $\rho$ *(g/cm$^3$)* | $u_p$ *(km/s)* | $\sigma$ *(GPa)* |
|---|---|---|---|---|---|---|---|
| Z-2096 | $Ta_2O_5$ | 1.256 | 11.26-11.20 | 13.37±0.62 | 3.81±0.47 | 8.97±0.11 | 150.5±6.1 |
| | WC | 8.870 | 9.78-9.98 | 8.77±0.10 | 23.20±0.74 | 5.41±0.07 | 421.0±6.1 |
| Z-2157 | $Ta_2O_5$ | 1.259 | 10.23-10.42 | 11.78±0.43 | 4.33±0.49 | 8.36±0.09 | 123.9±4.0 |
| | WC | 8.799 | 11.41-11.54 | 10.89±0.10 | 19.75±0.38 | 6.04±0.06 | 578.5±6.2 |

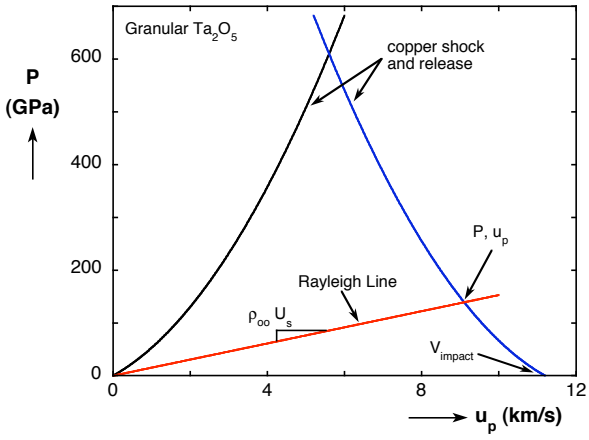


**Figure 10.** P-u diagram for impedance matching between Cu impactor and $Ta_2O_5$ sample.

This page intentionally left (almost) blank.

# 4 Results of 2-Stage Gas Gun Experiments

Planar impact experiments were conducted on the three varieties of $Ta_2O_5$ using the 2-stage gas gun to obtain shock data at pressures below those achieved on Z. The experimental configuration for these experiments was described in Section 2.3, and details of the experiments are given in Table 2.

In experiments in which the VISAR monitored the interface between the granular sample and the PMMA, the surface was rapidly degraded with the arrival of the shock and light return was quickly lost. This yields only a sharp signal corresponding to the shock arrival time. In contrast, those experiments incorporating LiF windows with Al buffers allowed the velocity to be measured for some length of time after shock arrival. The velocity history measured in this manner for a Cerac $Ta_2O_5$ sample is shown in Fig. 11. The four VISAR records from outside the sample are shown as abrupt rises in velocity just before 0.1 $\mu$s with the differences mainly due to tilt of the impactor. The differences in arrival time correspond to an impactor tilt on the order of 6 mrad. The shock arrives at the end of the first step very close to the same time for the two sides, around 0.23-0.24 $\mu$s, and the shock arrives at the back of the center step around 0.35 $\mu$s. The steady-state velocities achieved for the second (center) step agrees with one of the outer steps but is somewhat lower than the other. These second velocity states are discussed below. Because the LiF windows in these experiments were only about 6 mm in diameter, the velocities recorded are only indicative of uniaxial strain states for a limited time.

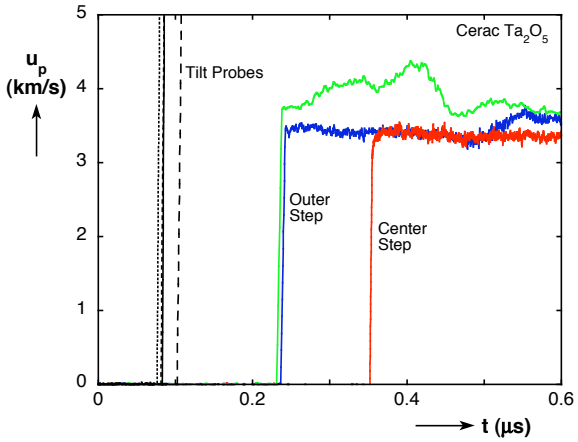


**Figure 11.** Velocity history records for 2-stage experiment $Ta_2O_5$-10 on Cerac material.

A representative velocity record for a consolidated $Ta_2O_5$ sample is shown in Fig. 12. The velocity measurements at the perimeter are abrupt velocity jumps giving the shock arrival time only. However, since the central window is larger in diameter, longer read time is possible and in this case the arrival of release wave from the back of the impactor is seen. In principal, it should be possible to use the velocity history of the unloading to calculate the release path as has been done previously for other ceramics [Reinhart and Chhabildas, 2003; Vogler et al., 2004, 2006]. However, because of the use of an impactor and driver that are of different materials than the sample, this is a complicated prospect and has not been completed.

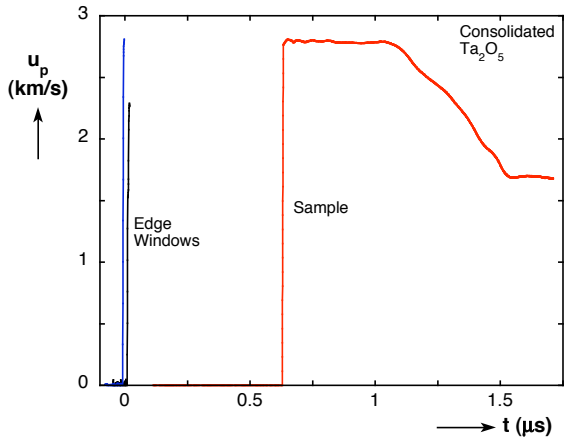


**Figure 12.** Velocity history records for 2-stage experiment $Ta_2O_5$-c8 on consolidated material.

The shock velocity for the powder samples is determined as a least squares fit to the distances between the driver plate and the steps of the target plotted against the shock arrival times. When Al buffers are present, the traversal time for them is accounted for using the known shock response of Al [Mitchell and Nellis, 1981]. In contrast to the low velocity compaction experiments [Brown et al., 2007; Vogler et al., 2007] the waves have no measurable rise time, so considering the arrival time at the driver/powder interface should introduce minimal error. In all cases, a very good fit was obtained for the shock velocity through the three measurement locations (driver/sample interface, first step, and second step). The procedure is the same for the consolidated sample except that there are only two measurement locations, the driver/sample interface and the back of the sample.

Once the shock velocity is determined, the Hugoniot state can be found using impedance matching and the known response of the driver material as discussed in the previous section. This is shown graphically with a so-called $P-u$ diagram in Fig. 13. Note that the release path for the driver material is assumed to be the reflected Hugoniot for the material, a reasonable approximation for the regime of these experiments [Nellis et al., 2003]. In addition to the Hugoniot state, a reshock state can be determined from the velocity measured with VISAR. A slight release occurs from the Al buffer to the LiF window, so both states are shown in the figure. Further calculations are required to determine the reshock states for the experiments.

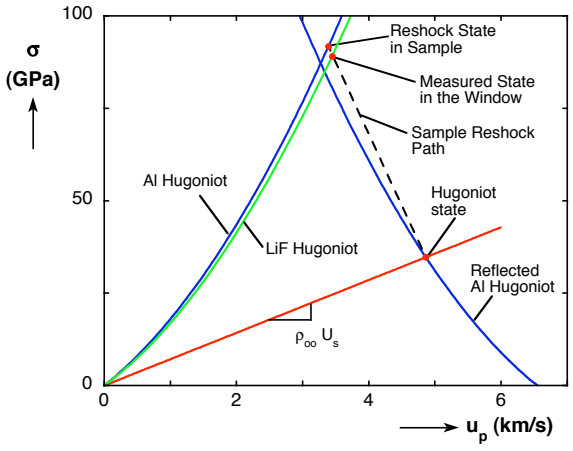


**Figure 13.** Impedance matching diagram in the P-$u_p$ plane for $Ta_2O_5$ showing the determination of the Hugoniot state and the reshock state of the material.

**Table 2.** Details of materials and Hugoniot states for 2-stage gas gun experiments.

| *Material* | *Shot* | $\rho_{oo}$ *(g/cm$^3$)* | *Impactor Material* | $V_{impact}$ *(km/s)* | $U_s$ *(km/s)* | $\rho$ *(g/cm$^3$)* | $u_p$ *(km/s)* | $\sigma$ *(GPa)* |
|---|---|---|---|---|---|---|---|---|
| Cerac $Ta_2O_5$ | $Ta_2O_5$-6 | 1.252 | Cu | 3.450 | 3.751 | 7.086 | 3.088 | 14.50 |
| | $Ta_2O_5$-7 | 1.139 | Cu | 4.624 | 5.115 | 5.567 | 4.068 | 23.70 |
| | $Ta_2O_5$-8 | 1.131 | Cu | 5.511 | 6.070 | 5.327 | 4.781 | 32.82 |
| | $Ta_2O_5$-9 | 1.117 | Cu | 6.743 | 7.731 | 4.314 | 5.729 | 49.47 |
| | $Ta_2O_5$-10 | 1.141 | Al | 6.550 | 6.257 | 5.125 | 4.864 | 37.73 |
| American Elements $Ta_2O_5$ | $Ta_2O_5$-11 | 2.721 | Al | 3.497 | 3.497 | 8.274 | 2.347 | 22.33 |
| | $Ta_2O_5$-12 | 3.017 | Al | 4.483 | 4.093 | 9.564 | 2.802 | 34.60 |
| | $Ta_2O_5$-13 | 3.070 | Al | 5.477 | 4.807 | 9.821 | 3.304 | 48.76 |
| | $Ta_2O_5$-14 | 3.203 | Al | 6.667 | 5.644 | 10.13 | 3.860 | 69.78 |
| Consolidated $Ta_2O_5$ | $Ta_2O_5$-c6 | 7.522 | Cu[1] | 1.847 | 3.672 | 10.91 | 1.141 | 31.51 |
| | $Ta_2O_5$-c7 | 7.412 | Cu[2] | 3.066 | 4.434 | 12.81 | 1.868 | 61.39 |
| | $Ta_2O_5$-c8 | 7.404 | Cu[1] | 4.046 | 5.352 | 13.39 | 2.393 | 94.80 |
| | $Ta_2O_5$-c9 | 7.358 | Cu[1] | 5.046 | 6.331 | 13.64 | 2.915 | 135.8 |

[1]includes Cu driver in front of sample
[2]sample impacted directly

This page intentionally left (almost) blank.

# 5 Hugoniot Results

## 5.1 $Ta_2O_5$

Hugoniot results from two Z experiments on Cerac $Ta_2O_5$ as well as 2-stage gas gun results on all three forms of the material are shown in Fig. 14. Because of the much greater dissipative heating that occurs at higher initial distentions, the data for the Cerac ( 1.2 g/cm$^3$) material have significantly lower densities than the AE ( 3.0 g/cm$^3$) and consolidated material. In fact, a negative slope in the curve for the Cerac material in the range of 10-50 GPa is seen. This phenomenon is sometimes referred to as anomalous compressibility and is well understood in the shock physics literature. The pressure states obtained on Z are more than 2.5 times the highest level attained with the 2-stage guns due to the higher flyer velocities, 10-11 vs. 6.5 km/s. As the initial density of the material increases, the top Hugoniot states increase commensurately. The highest data point for the Cerac material is somewhat anomalous in this regard since a copper impactor and driver were used for that shot while aluminum was used for the AE and consolidated materials.

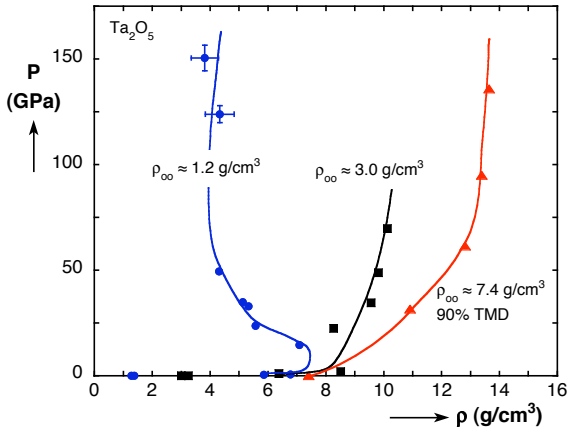


**Figure 14.** Hugoniot results for granular and consolidated $Ta_2O_5$. Curves are shown only to aid the eye

Recently the P-$\lambda$ model [Grady and Winfree, 2001; Grady et al., 2000], which was originally developed for porous materials and mixtures at low to moderate pressures, was extended to the high pressure regime where thermal effects become critical and materials can exhibit anomalous compressibility [Fenton et al., 2011]. The conventional approach of calculating the porous response based on an equivolume mapping from the reference curve will not work when the material exhibits anomalous compressibility since the mapping would be multi-valued. Instead, an equipressure mapping suggested by Rice and Walsh [1957] was utilized. Since no high-pressure data on fully dense $Ta_2O_5$ was available, an initial estimate for the response was made based on nanoindentation results [Buchheit and Vogler, 2010]. A value for the reduce modulus $E_r$ of 150 GPa was obtained from those experiments. Utilizing the relationship for bulk modulus of

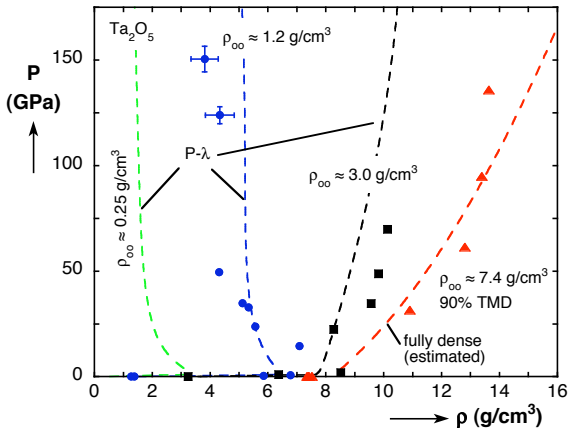


**Figure 15.** Hugoniot results from the P-$\lambda$ model (dashed lines) compared to experimental results for granular and consolidated $Ta_2O_5$.

$$K_o = \frac{E_r}{3(1-2\nu)(1-\nu^2)} \tag{1}$$

and assuming a value of 0.2 for $\nu$, which is a reasonable assumption for most ceramics, we find a value of 86.8 GPa for the bulk modulus $K_o$. From this, a value for the bulk sound speed of 3.3 km/s is obtained. This is used in the common linear $U_s - u_p$ relationship of

$$U_s = c_o + s u_p. \tag{2}$$

Although $c_o$ is not, in general, equal to the bulk sound speed, it is often very close to that value making it a reasonable assumption here. It is necessary to specify the thermal behavior of the material; here, that is done through the Grüneisen parameter $\Gamma$, which is assumed to have the form

$$\Gamma(P) = \Gamma_o e^{-(\frac{P}{K_o})^n} + \Gamma_\infty (1 - e^{-(\frac{P}{K_o})^n}). \tag{3}$$

Values of 1.15 and 0.5 are assumed for $\Gamma_o$ and $\Gamma_\infty$, respectively, and a value of unity is used for $n$. This gives a gradual decay of $\Gamma$ from 1.15 at ambient conditions to 0.5 at high pressures, the latter based upon the limiting case for very high pressures. As can be seen in Fig. 15, the model constructed in this manner fits the data quite well. The model results shown are not quite "blind" in that the value of $\Gamma$ was adjusted slightly to fit the data, but in some cases the ambient value might be available. If it were not, an assumption of $\Gamma_o = 1$ would be reasonable and, in this case, not much different from the results shown.

While the P-$\lambda$ results agree well with the Z and 2-stage results, there are additional data for $Ta_2O_5$ aerogel from the OMEGA laser facility [Miller et al., 2007]. These experiments were done for material with initial

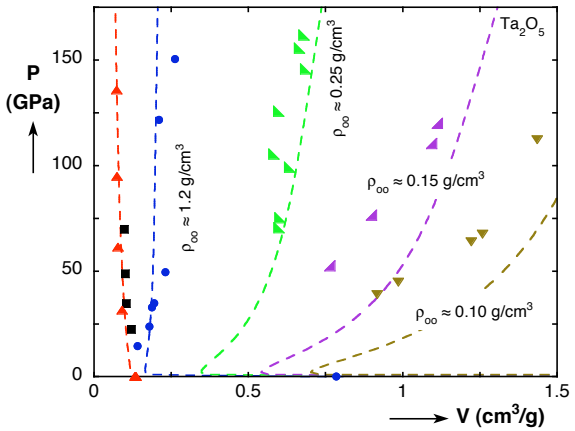


**Figure 16.** Hugoniot results from the P-$\lambda$ model (dashed lines) compared to experimental results for consolidated, granular, and aerogel [Miller et al., 2007] $Ta_2O_5$.

densities of 0.1, 0.15, and 0.25 g/cm$^3$, much lower than the Cerac material. The model predictions are shown in Fig. 16 along with the experimental results in the P-V plane to better emphasize the aerogel results. The model does a credible job of representing the data, though it seems to deviate more as the initial density decreases. It should be noted, however, that the re-analysis of these results using the revised quartz standard [Knudson and Desjarlais, 2009] is ongoing at LLNL and may shift the experimental data to agree better with the model results. Also, the EOS used assumes that the thermal properties of the material are only a function of pressure. This is likely to become an increasingly poor approximation for large initial distentions (low initial densities) such as the aerogel.

## 5.2 WC

The results from the two Z experiments for WC are shown in Fig. 17 along with a fit to the Hugoniot data from Trunin et al. [2001]. The LASL Hugoniot data [Marsh, 1980] for WC was taken for a material with 5% cobalt by weight and thus is not shown. Although the composition of the WC reported by Trunin et al. [2001] is not reported, their reported density of 15.66 g/cm$^3$ is actually slightly above the crystal density of WC, suggesting either a denser sintering aid than cobalt or a small amount of $W_2C$ was present. Also shown are the calculations for the P-$\lambda$ model following the outline above. It should be noted that the value of $\Gamma$ used in the model were based on a fit to a preliminary Hugoniot state for experiment Z-2096 (the lower pressure data point).

The most notable feature of the data is the inconsistency between the Hugoniot results for the two shots. Care should be taken in favoring one experimental result over another when lacking corroborating evidence. If the thermal properties of WC, about which there is significant uncertainty [Grady and Fenton, 2010], are varied by a relatively modest amount, one can capture either of the experimental points. However, no

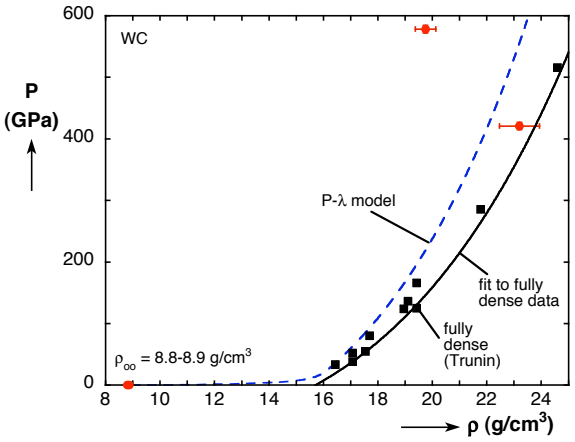


**Figure 17.** Hugoniot results for granular and fully dense WC along with results from the P-$\lambda$ model.

plausible model would be expected to be consistent with both data points.

Examination of the data reveals no obvious cause for the discrepancy: the initial densities are nearly the same, and the flyer velocities are measured accurately in both cases. Both rely upon the same copper response, but the granular WC is similar to copper in impedance so the Cu releases only a modest amount from the Hugoniot state. Since the Hugoniot of Cu is known quite well, only a minimal uncertainty arises from the response of copper. The most likely cause of the discrepancy is a problem in mounting the powder cell into the target, resulting in an offset between the quartz window and the impact surface of the cell as discussed in Section 3. Because of the construction of the target and the mounting of the VISAR probes, such a problem might not be detected. In previous experiments, offsets as large as 20 $\mu$m have been observed, but such an offset is not sufficient to bring the two points into agreement. To reconcile the differences between the two results, then, a much larger assembly issue must have occurred. Although it is possible that both experiments suffered from this but in a way that shifted the results in opposite directions, it seems more likely that only one of the experiments had a gross problem with assembly. If that is the case, then one would expect addition experimental data in this regime to corroborate one result or the other.

# 6 Summary and Conclusions

In this study, we have obtained high pressure shock results for granular ceramics using the Z machine and a 2-stage light gas gun to accelerate flyers to high velocities. The data for WC represent some of the highest pressure data reported in the literature for distended materials, while the data for $Ta_2O_5$ reaches high pressures for two initial densities and a nearly fully consolidated form of the material. The data on $Ta_2O_5$ is complemented by experiments from the literature [Miller et al., 2007] utilizing lasers that were performed on aerogels at three initial densities. In both the Z and gas gun experiments, stepped targets provide for accurate measurements of the shock velocities in the samples. Unfortunately, in many cases the VISARs did not return any data other than the time of shock arrival. For the 2-stage shots, this is largely due to issues associated with windows and the reflective surfaces on them. These issues were largely overcome by utilizing LiF windows with aluminum buffers. For the Z experiments, however, the quartz windows were expected to become reflective so that the shock velocity is measured directly. This did not occur, suggesting that irregularities in the shock front of the granular material imprinted themselves upon the shock in the window, thus reducing its reflectivity. Another technical approach may be needed in order to make these measurements possible.

The Z experiments revealed shortcomings in the experimental design that will be improved upon in the future. Namely, the impact of the flyer directly with the fiber probes does not provide an adequate fiducial of flyer impact. Also, failure to measure the offset of the impact surfaces of the quartz windows and the copper target introduce additional uncertainties. It may be that these uncertainties are responsible for the significant scatter that is seen in the WC data, but that is far from clear. Additional work is needed to determine the true high-pressure behavior of granular WC.

The P-$\lambda$ model has recently been extended to the high pressure regime for distended materials, and the data on $Ta_2O_5$ provide an excellent test of that capability. Initial calculations show that the model can do a good job of capturing the response of the material for a wide range of distentions including very low density aerogels.

Finally, the usefulness of nanoindentation for developing an EOS when lacking other data has been demonstrated. Based solely on nanoindentation of individual grains of the ceramic, a credible first order estimate of the EOS of $Ta_2O_5$ is shown to be possible. While one would not expect an EOS constructed in this manner to correctly capture all the subtleties of the behavior of a material, it would certainly be better than nothing and would require only a very modest amount of experimental effort.

This page intentionally left (almost) blank.

# References


Barker, L.M., Hollenbach, R.E., 1972. Laser interferometry for measuring high velocities for any reflecting surface. Journal of Applied Physics 43, 4669–4675.

Borg, J.P., Vogler, T.J., 2008. Mesoscale calculations of the dynamic behavior of a granular ceramic. International Journal of Solids and Structures 45, 1676–1696.

Borg, J.P., Vogler, T.J., 2009. Aspects of simulating the dynamic compaction of a granular ceramic. Modelling and Simulation in Materials Science and Engineering 17, 045003.

Brown, J.L., Vogler, T.J., Grady, D.E., Reinhart, W.D., Chhabildas, L.C., Thornhill, T.F., 2007. Dynamic compaction of sand. In: Elert, M., Furnish, M.D., Chau, R., Holmes, N., Nguyen, J. (Eds.), Shock Compression of Condensed Matter-2007. AIP, New York, pp. 1363–1366.

Buchheit, T.E., Vogler, T.J., 2010. Measurement of ceramic powders using instrumented indentation and correlation with their dynamic response. Mechanics of Materials 42, 599–614.

Davis, J.-P., 2006. Experimental measurement of the principal isentrope for aluminum 6061-T6 to 240 GPa. Journal of Applied Physics 99, 103512.

Fenton, G., Grady, D.E., Vogler, T.J., 2011. Intense shock compression of porous solids: application to WC and $Ta_2O_5$. In: Elert, M.L., Buttler, W.T., Vogler, T.J., Borg, J.P., Jordan, J.L. (Eds.), Shock Compression of Condensed Matter - 2011. AIP, (in press).

Grady, D.E., Fenton, G., 2010. Temperature states in the shock compression of granular powders with application to tungsten carbide. Applied Research Associates, Report.

Grady, D.E., Winfree, N.A., 2001. A computational model for polyurethane foam. In: Staudhammer, K.P., Murr, L.E., Meyers, M.A. (Eds.), Fundamental Issues and Applications of Shock-Wave and High-Strain-Rate Phenomena. Elsevier, New York, pp. 485–491.

Grady, D.E., Winfree, N.A., Kerley, G.I., Wilson, L.T., Kuhns, L.D., 2000. Computational modeling and wave propagation in media with inelastic deforming microstructure. Journal de Physique IV 10, 15–20.

Hall, C.A., Asay, J.R., Knudson, M.D., Stygar, W.A., Spielman, R.B., Pointon, T.D., Reisman, D.B., Toor, A., Cauble, R.C., 2001. Experimental configuration for isentropic compression of solids using pulsed magnetic loading. Review of Scientific Instruments 72, 3587–3595.

Hibbard, R.L., Bono, M.J., 2005. An overview of the target fabrication operations at Lawrence Livermore National Laboratory. Lawrence Livermore National Laboratory, Report UCRL-PROC-210896.

Hund, J.F., Paguio, R.R., Frederick, C.A., Nikroo, A., Thi, M., 2006. Silica, metal oxide, and doped aerogel development for target applications. Fusion Science and Technology 49, 660–675.

Knudson, M.D., Asay, J.R., Deeney, C., 2005. Adiabatic release measurements in aluminum from 240 to 500 GPa states on the principal Hugoniot. Journal of Applied Physics 97, 073514.

Knudson, M.D., Desjarlais, M.P., 2009. Shock compression of quartz to 1.6 TPa: redefining a pressure standard. Physical Review Letters 103, 225501.

Knudson, M.D., Hanson, D.L., Bailey, J.E., Hall, C.A., Asay, J.R., 2001. Equation of state measurements in liquid deuterium to 70 GPa. Physical Review Letters 87, 225501.

Lassner, E., Schubert, W.-D., 1999. Tungsten: Properties, Chemistry, Technology of the Element, Alloys, and Chemical Compounds. Kluwer Academic / Plenum Publishers, N.Y.

Marsh, S.P., 1980. LASL Shock Hugoniot Data. University of California Press, Berkeley.

Miller, J.E., Boehly, T.R., Meyerhofer, D.D., Eggert, J.H., 2007. Equation-of-state measurements in $Ta_2O_5$ aerogel. In: Elert, M., Furnish, M.D., Chau, R., Holmes, N., Nguyen, J. (Eds.), Shock Compression of Condensed Matter - 2007. American Institute of Physics, pp. 71–74.

Mitchell, A.C., Nellis, W.J., 1981. Shock compression of aluminum, copper, and tantalum. Journal of Applied Physics 52, 3363–3374.

Nellis, W.J., Mitchell, A.C., Young, D.A., 2003. Equation-of-state measurements for aluminum, copper, and tantalum in the pressure range 80-440 GPa (0.8-4.4 Mbar). Journal of Applied Physics 93, 304–310.

Reinhart, W.D., Chhabildas, L.C., 2003. Strength properties of Coors AD995 alumina in the shocked state. International Journal of Impact Engineering 29, 601–619.

Rice, M.H., Walsh, J.M., 1957. Equation of water to 250 kilobars. The Journal of Chemical Physics 26, 824–830.

Root, S., Magyar, R.J., Carpenter, J.H., Hanson, D.L., Mattson, T.R., 2010. Shock compression of a fifth period element: liquid xenon to 840 GPa. Physical Review Letters 105, 085501.

Trunin, R.F., Gudarenko, L.F., Zhemokletov, M.V., Simakov, G.V., 2001. Experimental Data on Shock Compression and Adiabatic Expansion of Condensed Matter. Russian Federal Nuclear Center - VNIIEF, Sarov, Russia.

Trunin, R.F., Simakov, G.V., Sutulov, Y.N., Medvedev, A.B., Rogozkin, B.D., Fedorov, Y.E., 1989. Compressibility of porous metals in shock waves. Soviet Physics JETP 69, 580–588.

Vogler, T.J., Alexander, C.S., Thornhill, T.F., Reinhart, W.D., 2011. Pressure-shear experiments on granular materials. Sandia National Laboratories, Report SAND2011-6700.

Vogler, T.J., Lee, M.Y., Grady, D.E., 2007. Static and dynamic compaction of ceramic powders. International Journal of Solids and Structures 44, 636–658.

Vogler, T.J., Reinhart, W.D., Chhabildas, L.C., 2004. Dynamic behavior of boron carbide. Journal of Applied Physics 95, 4173–4183.

Vogler, T.J., Reinhart, W.D., Chhabildas, L.C., Dandekar, D.P., 2006. Hugoniot and strength behavior of silicon carbide. Journal of Applied Physics 99, 023512.

# DISTRIBUTION:

1 Tarabay Antoun
Lawrence Livermore National Laboratory
7000 East Avenue
Livermore, CA 94550

1 Jon Eggert
Lawrence Livermore National Laboratory
7000 East Avenue
Livermore, CA 94550

1 Don Fujino
Lawrence Livermore National Laboratory
7000 East Avenue
Livermore, CA 94550

1 Amy Lazicki
Lawrence Livermore National Laboratory
7000 East Avenue
Livermore, CA 94550

1 Phil Sterne
Lawrence Livermore National Laboratory
7000 East Avenue
Livermore, CA 94550

1 Darcie Dennis-Koller
Los Alamos National Laboratory
P.O. Box 1663
Los Alamos, NM 87545

1 D. Anthony Fredenburg
Los Alamos National Laboratory
P.O. Box 1663
Los Alamos, NM 87545

1 Rick Martineau
Los Alamos National Laboratory
P.O. Box 1663
Los Alamos, NM 87545

1 David Robbins
Los Alamos National Laboratory
P.O. Box 1663
Los Alamos, NM 87545

1 Gregg Fenton
Applied Research Associates
4300 San Mateo Blvd., Suite A-220
Albuquerque, NM 87110

1 Dennis Grady
Applied Research Associates
4300 San Mateo Blvd., Suite A-220
Albuquerque, NM 87110

| | | | |
|---|---|---|---|
| 10 | MS | 9042 | T.J. Vogler, 8246 |
| 1 | MS | 9042 | Chris Moen, 8246 |
| 1 | MS | 9154 | Mary Gonzales, 8240 |
| 1 | MS | 1186 | M. Herrmann, 1640 |
| 1 | MS | 1106 | T. Ao, 1646 |
| 1 | MS | 1195 | C.S. Alexander, 1646 |
| 1 | MS | 1195 | J. Brown, 1646 |
| 1 | MS | 1195 | J.-P. Davis, 1646 |
| 1 | MS | 1195 | Daniel Dolan, 1646 |
| 1 | MS | 1186 | Dawn Flicker, 1646 |
| 1 | MS | 1195 | M.D. Furnish, 1646 |
| 1 | MS | 1195 | M.D. Knudson, 1646 |
| 1 | MS | 1195 | G.T. Leifeste, 1647 |
| 1 | MS | 1195 | W.D. Reinhart, 1646 |
| 1 | MS | 1195 | J. Robbins, 1646 |
| 1 | MS | 1195 | S. Root, 1646 |
| 1 | MS | 1195 | T.F. Thornhill, 1647 |
| 1 | MS | 1195 | J.L. Wise, 1646 |
| 1 | MS | 1189 | M. Desjarlais, 1640 |
| 1 | MS | 1205 | C.A. Hall, 5947 |
| 1 | MS | 0899 | Technical Library, 9536 (electronic copy) |

Sandia National Laboratories